High vulnerability and exposure main driver behind Kinshasa's deadly floods following heavy, but not unusual rainfall

Authors

Joyce Kimutai, *Centre for Environmental Policy, Imperial College, London, UK*
Dieudonne Nsadisa Faka*, The intra-ACP Climate Services Programme of The Organisation of African, Caribbean and Pacific States, Democratic Republic of the Congo*
Prosper Ayabagabo, *Rwanda Meteorology Agency, Kigali, Rwanda*
Hubert Kabengela*, Prévisionniste Météo, Democratic Republic of the Congo*
Mariam Zachariah, *Centre for Environmental Policy, Imperial College, London, UK*
Friederike Otto, *Centre for Environmental Policy, Imperial College, London, UK*
Dora Vrkić, *Grantham Institute - Climate Change and the Environment, Imperial College London, London, UK*
Sarah Kew, *Royal Netherlands Meteorological Institute (KNMI), De Bilt, The Netherlands*
Izidine Pinto, *Royal Netherlands Meteorological Institute (KNMI), De Bilt, The Netherlands*
Maja Vahlberg, *Red Cross Red Crescent Climate Centre, The Hague, the Netherlands; Swedish Red Cross, Stockholm, Sweden (based in Ubmeje/Umeå, Sweden)*
Karina Izquierdo, *Red Cross Red Crescent Climate Centre, The Hague, the Netherlands (based in Mexico City, Mexico)*
Nick Baumgart, *Copenhagen Centre for Disaster Research, Global Health Section, Department of Public Health, University of Copenhagen, Copenhagen, Denmark*
Emmanuel Raju, *Copenhagen Centre for Disaster Research, Global Health Section, Department of Public Health, University of Copenhagen, Copenhagen, Denmark; African Centre for Disaster Studies, North-West University, South Africa*

Review authors

Sjoukje Philip, *Royal Netherlands Meteorological Institute (KNMI), De Bilt, The Netherlands*
Roop Singh, *Red Cross Red Crescent Climate Centre, The Hague, The Netherlands (based in New Jersey, USA)*
Matthieu Kiansumba, *DRC Red Cross, Kinshasa, Democratic Republic of the Congo*
Admire Nyathi, *Kinshasa Cluster Delegation, International Federation of Red Cross and Red Crescent Societies (IFRC), Brazzaville, Republic of the Congo*
Paloma Diaz de Durana, *Swedish Red Cross, Stockholm, Sweden (based in Kinshasa, DRC)*

Main findings

- Kinshasa is prone to frequent and deadly flooding during the rainy season (October to May). It is built next to the Congo River and several rivers run directly through the city, including the Ndjili. With close to 18 million residents, Kinshasa is one of the most populated cities in the world. Around 70% of the urban population lives in dense informal housing, much of it in areas prone to floods and landslides. In 2022, more than 100 people died following a similarly heavy downpour.
- From a hazard point of view, the event as observed in 2025 is not rare. Similar periods of heavy rainfall are expected to occur on average every second year in today's climate, which has been warmed by 1.3°C, due to the burning of fossil fuels.
- To assess whether such heavy rainfall events would have been more or less frequent in the past we assess three gridded data products, as well as two weather stations located in Kinshasa. All three gridded datasets show very different trends, including one that suggests climate change made the event much more likely, while two show no change. The station data is only available until 2023, so does not include the event, but shows different events and trends in the overlapping years than all three gridded products.
- Climate models also show very varying trends, including a strong increase, no trends and a decreasing trend in heavy precipitation over the region since the pre industrial climate. However, this is no indication that there is no trend, as the discrepancies are very high.
- The scarcity and inaccessibility of meteorological data, as well as inadequate performance of climate models means that we cannot confidently evaluate the role of climate change in the rainfall that led to flooding. Our previous study on a 2023 flood in Eastern DRC was similarly inconclusive for the same reasons, highlighting an ongoing need to invest in weather monitoring stations and climate science to understand changing weather extremes in Central Africa.
- The IPCC projects an increase in heavy rainfall across Central Africa, particularly over short timescales of five days or less. Several data sources—including two weather stations—and about half of the climate models analyzed indicate a notable rise in heavy rainfall for both Kinshasa and the broader study region. Therefore, a future increase in heavy rainfall due to climate change is a strong possibility.
- Since gaining independence in 1960, the Democratic Republic of the Congo (DRC) has faced decades of political instability and conflict. Despite being one of the most mineral-rich countries in the world—with over half of the global cobalt supply, a key element in batteries and the global transition to renewable energy—the DRC remains the fourth poorest country globally.
- Prolonged conflict, particularly in the eastern regions (see WWA's other study in the DRC), continues to severely impact the country. In recent months, violence has intensified, resulting in thousands of deaths and displacing nearly seven million people. These ongoing crises in the east could have far-reaching ripple effects, such as increasing migration flows into cities.
- Floods in Kinshasa, which occur frequently and often result in high death tolls, highlight the urgent need to build resilience to heavy rainfall events. This urgency is further amplified by the city's rapid growth: Kinshasa's population is projected to double to nearly 40 million within the next 20 years.

- Flood risk is amplified by rapid population growth, limited infrastructure coverage, and high reliance on informal systems - particularly in areas where critical services such as drainage, healthcare, and electricity remain inconsistent or difficult to access. Drainage is frequently blocked by waste pollution, and there is limited waste management services and sewage maintenance, increasing flooding.
- While progress is being made, for example, the drafting of a new law on the DRC's town planning and construction code that could reduce flood exposure, more comprehensive efforts are needed to reduce the impacts of very devastating, but common floods. Adaptation finance will be critical to support the country's flood adaptation measures as population growth in Kinshasa and surrounding cities continues.

1 Introduction

The torrential rains between April 4 and 7, Kinshasa—the capital of the Democratic Republic of the Congo (DRC)—caused severe flooding, landslides and silting that resulted in significant casualties and damage. However, the local station (Ndjili) reported around 75.2 mm of rainfall at the Airport on a single event that started on the night of 4th April 2025 going to the morning of 5th April 2025. The disaster was triggered when the N'Djili and Nsuenge rivers east of the city, which runs through the city of approximately 17.8 million people, burst its banks on April 5–6, submerging major roads and hundreds of buildings (Aljazeera, 2025). The bridge over the Ndjili River in Debonhomme was submerged by up to 3 meters, rendering it impassable. Homes near the river and in surrounding neighborhoods were inundated, with private boats used for evacuations. To note is that, the river's rising levels were partly due to upstream runoff from Central Kongo Province, even in the absence of local rainfall. As of April 7, at least 33 people had been reported dead, 46 injured, 1,425 displaced and 3,450,412 affected as reported by the Kinshasa Provincial government. Thirteen (Matete, Kisenso, Ngaba, Limete, Mont Ngafula, Ndjili, Kalamu, Bumbu, Ngaliema, Selembao, Makala, Lemba and Masina) of Kinshasa's 24 municipalities were affected, with flooding cutting off access to over half of the city (MSN, 2025). In addition, there were several silted up houses which led to much vulnerability of communities.

The floods also damaged critical infrastructure, including the main road to the airport—which links Kinshasa to the rest of the country. Access to clean drinking water has been disrupted in at least 16 communes, as water facilities were impacted by the floodwaters. In response, the government established at least four emergency shelters, which housed hundreds of displaced families. This latest disaster comes as the country continues to face a major humanitarian crisis in its eastern region, more than 2,600 kilometers from Kinshasa, where ongoing conflict with M23 rebels has displaced hundreds of thousands (Aljazeera, 2025). It also follows a similarly devastating flood event in 2022, which claimed the lives of at least 100 people in Kinshasa (IFRC, 2022).

Kinshasa has a hot, humid tropical climate with a rainy season extending from late September to late May. Peak rainfall typically occurs in November and April, with an annual average of over 100 rainy days. The heaviest downpours (over 50 mm) are concentrated in March, April, and November—accounting for more than half of the year's extreme rain events. November is usually the wettest month, often preceding peak water levels in the Congo River. The city's geography—situated in a lowland plain surrounded by hills—contributes to significant runoff during heavy rains, especially on its asphalt-covered surfaces. Rainfall is influenced by both regional and local atmospheric

dynamics. Moisture-laden southwest monsoon winds, entering from the Gulf of Guinea, gain humidity from rivers and lakes as they pass through Equateur and Bandundu provinces before reaching Kinshasa. Southeastern trade winds also pick up moisture over Bandundu, with both wind systems converging over Kinshasa to produce thunderstorms and intense rainfall. Local weather is further shaped by thermal contrasts between the Congo River, surrounding plains, and nearby hills. These differences generate convective movements and breezes that lead to cloud formation and afternoon thunderstorms, particularly around 4 PM when temperatures peak. Despite broad seasonal patterns, rainfall across Kinshasa can be highly localized due to complex convection zones. Studies have shown that it may rain in one part of the city while another remains dry. Multiple sources of convection—including airflows from Brazzaville, synoptic squall lines, and systems from Angola—contribute to this variability. Additionally , the rainfall is influenced by the interactions between Indian and Atlantic Ocean moisture influx through the Mascarene and St Helena quasi permanent anticyclones respectively. The moisture influx enters the DRC over the east from the Indian Ocean and over the west from the Atlantic Ocean. In addition, the Madden Julian Oscillations (MJO) as well as the Congo forest play a big role in local circulations and enhanced rainfall at intraseasonal timescale. The cyclic MJO with a period reaching to 45 days modulates both the March-May and September - December over the country.

Between 1986 and 2024, Kinshasa/N'Djili station recorded an average of 1,530 mm of rain annually over approximately 112 rainy days. Most rainfall (about 70%) occurs in the form of thunderstorms, often with damaging intensity. In recent decades, Kinshasa has experienced numerous extreme rainfall events resulting in severe flooding, landslides, and loss of life. Notable events include the deadly floods of 1961–62, 1973, 1990, 1994, 2001, and most recently in January 2022, when electrocution from a downed power line highlighted the risks posed by intense storms. These recurrent events underscore the growing threat of extreme rainfall to lives, infrastructure, and economic stability in the city and across the DRC.

1.1 Rainfall Extremes in Central Africa

Central Africa, home to the Congo Basin—the world's second-largest river basin and rainforest after the Amazon—is also known for the planet's most intense thunderstorms. According to IPCC, 2021, DRC has observed an increase in heavy rainfall since the 1950s, with low confidence (due to limited agreement) in human contribution to the observed change. Between 1979 and 2014, a significant drying trend was observed in the April–May–June (AMJ) rainfall season. However, a return to wetter conditions was recorded during 2016–2020, comparable to the earlier wet phase of 1979–1993 (Nicholson et al., 2022). Interestingly, the meteorological drivers behind these two wet periods differed. The 1979–1993 wet phase was linked to changes in the tropical Walker circulation, moisture flux dynamics, and Pacific sea surface temperatures (SSTs), characterized by a warmer central/eastern Pacific and a cooler western Pacific. This produced a weaker-than-average trans-Pacific SST gradient. In contrast, the 2016–2020 wet period occurred during generally higher SSTs across the Pacific compared to both earlier phases (Nicholson et al., 2022). In northeastern DRC, the annual rainfall shows a slight upward trend overall, with seasonal increases during March–May (MAM) and August–November (ASON), while little to no change was observed during December–February (DJF)

and June–July (JJ) (Posite et al., 2024). Future Projections indicate increases in total precipitation are expected in the north, east, and western edges of the Congo Basin, regardless of scenario or time period. This is partly attributed to intensified zonal moisture divergence in the upper atmosphere. However, along the wetter Guinea Coast and much of Central Africa, models suggest only minor changes in total rainfall but a reduction in the duration of wet spells.

1.2 Data gaps and inconsistencies in gridded observational products

Accurately quantifying changes in precipitation and its associated uncertainty remains a challenge, particularly across the Central African region, where rain gauge networks are sparse and unevenly distributed. Most of these stations are typically situated in urban areas, airports, or along major roads, with very few located in rural regions (Dinku, 2019). Generally, there has been a significant decline in reported rainfall measurements across the continent in the recent past (Muthoni, 2020). Notably, during the early 2010s, weather station reports from much of the DRC—which spans over 2 million km²—were no longer transmitted to the Global Telecommunication System, leading to huge data gaps. New advancements in science and technology have enable development of several global satellite and reanalysis-based rainfall products, aimed at addressing the limitations of in situ gauge observations. However these products differ widely in terms of their underlying algorithms, input data sources, latency, record length, spatial and temporal resolution, and intended applications (Mekonnen et al., 2023). Mekonnen et al. (2023) notes that no single rainfall product consistently performs well across all temporal and spatial scales. As expected, rain gauge-merged products contain smaller error compared to the satellite-only products (McCollum et al., 2000; Awange et al., 2016). Intercomparison studies by Awange et al., 2015 and Camberlin et al, 2019 on seven satellite-based gridded rainfall products—ARC, CHIRPS, CMORPH, PERSIANN, TAPEER, TARCAT, and TMPA—was conducted over Central Africa against 154 daily rain-gauge stations compiled from global datasets, national meteorological services, and monitoring initiatives show that on average, MSWEP, IMERG, and CHIRPS showed strong performance at the daily timescale—in that order—while RFE, ARC, and CHIRPS were more reliable at monthly and annual scales. Figure 1 shows the time series of maximum cumulative 7-day rainfall from station observations, ERA5, CHIRPS, and TAMSAT. The results show clear discrepancies among the datasets, indicating limited agreement.

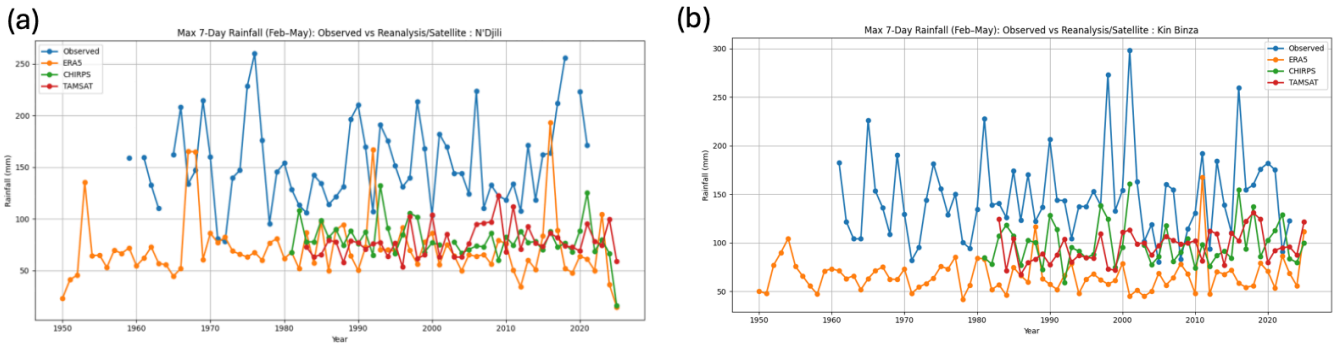

Figure 1. *Maximum cumulative 7-day rainfall as depicted by station observations at two locations in Kinshasa city in DRC (a) N'Djili and (b) Binza, along with the respective estimates at the nearest*

grid from the reanalysis and satellite products used in the study, namely, ERA5, CHIRPS, and TAMSAT.

1.3 Event Definition

Kinshasa (see red dot in Figure 2), located in a low-lying plain surrounded by hills and drained by numerous local rivers—including the Nsele and Ndjili, both major tributaries of the Congo River—experienced the most severe impacts from the rainfall event. However, the heavy rainfall extended beyond the city, affecting the surrounding and central regions of the Democratic Republic of the Congo. The N'Djili river basin spans approximately 2,000 km² (15°9'–15°39'E, 4°22'–4°59'S) from the Central Kongo province to the city of Kinshasa (Luboya, 2002). It consists of two distinct sections, an upper course encompassing the rural territories of Kasangulu and Madimba, and a lower course covering about 625 km² (about 31.2% of the basin) that feeds the city of Kinshasa.. The N'Djili river originates in the hills of Bas-Congo and flows south to north through Kinshasa, emptying into the Congo River in a delta with anastomosing arms. It forms a natural boundary between eastern Kinshasa and the rest of the city, alongside the N'sele River, delineating an arc-shaped plain 4 to 6 km wide. The riverbanks, now heavily urbanized, support dwellings, market gardens, and livestock farms. The alluvial valleys of the N'Djili system, namely, Lukaya, Matete, Kwambila, Imbu, Bimunsaka, and Kimbasala, play a vital economic role in agriculture and urban development. Therefore to better capture the rainfall associated with the widespread flooding, we focused our analysis on river basins in and around Kinshasa, extending into the central part of the country (see red outline in Figure 2).

Given that flood events can be triggered by either short-duration, high-intensity rainfall leading to flash floods, or by prolonged multi-day rainfall causing flooding through soil saturation, we examine the maximum consecutive 7-day rainfall during the February–May (FMAM) season (hereafter Feb-May RX7day) to capture a range of flood-inducing rainfall processes. The study region used is relatively homogeneous in both elevation and climatological characteristics (not shown).

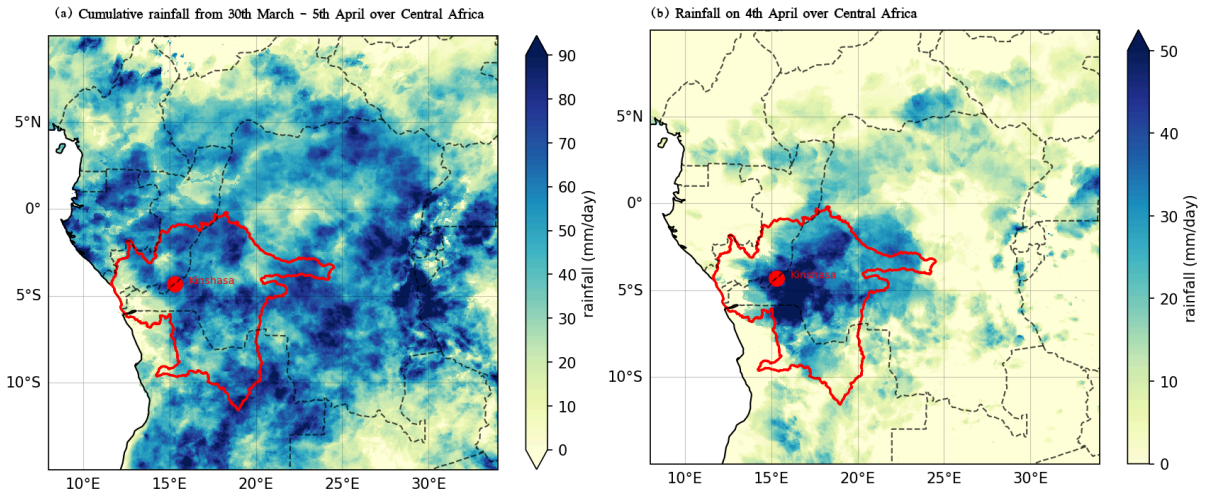

Figure 2. *(a) 7- day (30th March - 5th April) cumulative rainfall over Central Africa region, encompassing the Democratic Republic of Congo; (b) Rainfall on the 4th of April over region based TAMSAT dataset. The red outline shows the study region.*

In this report, we study the influence of anthropogenic climate change by comparing the likelihood and intensity of similar Feb-May RX7day values at present with those in a 1.3 °C cooler climate. We also extend this analysis into the future by assessing the influence of a further 1.3 °C of global warming from present. This is in line with the latest Emissions Gap Report from the United Nations Environment Programme, which shows that the world is on track for at least 2.6 °C temperature rise given currently implemented policies (UNEP, 2024).

2 Data and methods

2.1 Observational data

We utilise daily data for three gridded observational datasets and two in situ stations :
(i) **Climate Hazards Group InfraRed Precipitation with Station data (CHIRPS)**. CHIRPS (Climate Hazards Group InfraRed Precipitation with Station data; Funk et al., 2015b). CHIRPS is the state of the art observational daily dataset developed by the UC Santa Barbara Climate Hazards Group called "Climate Hazards Group InfraRed Precipitation with Station data" available for the period 1981–present. For this dataset, we utilised daily rainfall data from 1981-2024.

(ii) **Tropical Applications of Meteorology using SATellite and ground based observations (TAMSAT)**. TAMSAT is a daily rainfall dataset based on high-resolution thermal-infrared observations generated by breaking down 5-day total TAMSAT rainfall estimates into daily increments, achieved through the utilisation of daily cold cloud duration information. We used the daily rainfall dataset available from 1983 to the present.
(iii) **ERA5 (5th Generation product from the European Centre for Medium-Range Weather Forecasts (ECMWF)**. ERA5 reanalysis product begins in the year 1950 (Hersbach et al., 2020). We use monthly rainfall, maximum and minimum temperature from this product. It should be noted that the variables from ERA5 are not directly assimilated, but these are generated by atmospheric components of the Integrated Forecast System (IFS) modelling system. Due its low performance in the pre-satellite period, we utilised only data from 1983 onwards from this dataset
(iv) **Weather Station data** from NDjili and Binza meteorological stations located at 15°26' E 4°23' S and 15° 15' E 04° 22' S, respectively and available from 1961 to 2023.

All gridded datasets were used to define the event, assess model performance, and carry out the attribution analysis. For consistency across gridded datasets, we use data spanning from 1983 to 2025, aligning with the start year of the TAMSAT record. As a measure of anthropogenic climate change we use the (low-pass filtered) global mean surface temperature (GMST), where GMST is taken from the National Aeronautics and Space Administration (NASA) Goddard Institute for Space Science (GISS) surface temperature analysis (GISTEMP, Hansen et al., 2010 and Lenssen et al. 2019).

2.2 Model and experiment descriptions

We use two multi-model ensembles from climate modelling experiments using very different framings (Philip et al., 2020): Sea Surface temperature (SST) driven global circulation high resolution models, coupled global circulation models and regional climate models.

1. **Coordinated Regional Climate Downscaling Experiment (CORDEX)-Africa (0.44° resolution, AFR-44)** multi-model ensemble (Nikulin et al., 2012), comprising of 18 simulations resulting from pairings of 10 Global Climate Models (GCMs) and 6 Regional Climate Models (RCMs). These simulations are composed of historical simulations up to 2005, and extended to the year 2100 using the RCP8.5 scenario.
2. **HighResMIP SST-forced model** ensemble (Haarsma et al. 2016), the simulations for which span from 1950 to 2050. The SST and sea ice forcings for the period 1950-2014 are obtained from the 0.25° x 0.25° Hadley Centre Global Sea Ice and Sea Surface Temperature dataset that have undergone area-weighted regridding to match the climate model resolution. For the 'future' time period (2015-2050), SST/sea-ice data are derived from RCP8.5 (CMIP5) data, and combined with greenhouse gas forcings from SSP5-8.5 (CMIP6) simulations. Sixteen models were evaluated for this study.

2.3 Statistical methods

Methods for observational and model analysis and for model evaluation and synthesis are used according to the World Weather Attribution Protocol, described in Philip et al., (2020), with supporting details found in van Oldenborgh et al., (2021), Ciavarella et al., (2021), Otto et al., (2024) and here. The key steps, presented in sections 3-6, are: (3) trend estimation from observations; (4) model validation; (5) multi-method multi-model attribution; and (6) synthesis of the attribution statement. In this report we analyse Feb-May RX7day averaged over the study region red-outlined in figure 2. For each time series we calculate the return period and intensity of the event under study for the 2025 GMST and for 1.3 C cooler GMST. This allows us to compare the climate of now and of the preindustrial past (1850-1900, based on the Global Warming Index), by calculating the probability ratio (PR; the factor-change in the event's probability) and change in intensity of the event.

A nonstationary generalised extreme value (GEV) distribution is used to model the Feb-May RX7day. For precipitation, the distribution is assumed to scale exponentially with the covariates, with the dispersion (the ratio between the standard deviation and the mean) remaining constant over time. This formulation reflects the Clausius Clapeyron relation, which implies that precipitation scales exponentially with temperature (Trenberth et.al., 2003, O'Gorman and Schneider 2009). The statistical models are estimated as follows. The variable of interest is assumed to follow a GEV distribution in which the location and scale parameters vary with GMST:

$$X \sim GEV(\mu, \sigma, \xi \mid \mu_0, \sigma_0, \alpha, T),$$

where X denotes the variable of interest, annual maxima of precipitation; T is the smoothed GMST; μ_0, σ_0 and ξ are the location, scale and shape parameters of the nonstationary distribution; and α is the trend due to GMST. As a result, the location and scale of the distribution have a different value in each year, determined by the GMST states. Maximum likelihood estimation is used to estimate the model parameters, with

$$\mu = \mu_0 exp\left(\frac{\alpha T}{\mu_o}\right) \quad \text{and} \quad \sigma = \sigma_0 exp\left(\frac{\alpha T}{\mu_o}\right).$$

For each time series we calculate the return period and intensity of the event under study for the 2025 GMST and for 1.3 C cooler GMST: this allows us to compare the climate of now and of the preindustrial past (1850-1900, based on the Global Warming Index), by calculating the probability ratio (PR; the factor-change in the event's probability) and change in intensity of the event.

3 Observational analysis: return period and trend

3.1 Analysis of point station data and gridded data

We estimate the return period of the 2025 event (Table 3.1) by fitting the statistical model described in 2.3 above to each observational time series shown in figure 1. The datasets show a wide range of estimates for probability ratio and intensity change. For return periods, the datasets give an estimate of roughly 2 years (1.58 in TAMSAT; 2.48 in ERA5). This suggests that under the global warming level, heavy rains such as this one are expected to happen in today's world about once every 2 years. It is worth noting that for CHIRPS and stations, in which the data do not cover the event (i.e., upto 2024 for CHIRPS and 2023 for stations), we estimate the magnitude of the events using the 2-year return period in the climate of 2025. Additionally, we use this same return period to assess changes in models. For changes in magnitudes, TAMSAT gives statistically significant increases and intensity i.e., 28% with lower bound of 18.69 and upper bound of 40.63%; while ERA5 and station data give almost no change i.e., 0.10 % (lower bound -16.10 upper bound 18.06), and positive increase albeit not statistically significant18.649 % (lower bound -15.106 upper bounds 70.399) and 8.79 % (lower bound -21.94 upper bound 42.69) respectively. CHIRPS shows a significant reduction in rainfall intensity. Overall, while we cannot definitively state that the heavy rainfall experienced in DRC between February and May 2025 is intensifying under the current climate, there is a strong possibility that climate change is increasing heavy rainfall in the region.

Table 3.1: *Estimated return periods, change in probability ratio and magnitude of Feb-March Rx7day events over the study region in the three reanalysis datasets and two stations in the high-impact area (around Kinshasa). Blue shading indicates an increasing trend (thick blue for statistically significant increasing trends) while orange indicates a decreasing trend.*

Dataset	Event		GMST (Covariate)	
	Magnitude (mm)	Return period (95% C.I.)	Probability Ratio (95% C.I.)	Change in magnitude (%) (95% C.I.)
TAMSAT	103.41	1.58 (1.06.. 2.66)	70.438 (9.8105 ... inf)	28.16 (18.69.... 40.63)
ERA5	82.518	2.48 (1.36 ... 13.37)	1.0125 (0.087 ... inf)	0.10 (-16.10.. 18.06)
CHIRPS	74.060	1.24 (1.02 ... 1.79)	0.80 (0.55 ... 0.99)	-11.82 (-21.86 ... -0.65)
N'Djili	164.84	2	1.95	18.649

Station		(1.25..4.95)	(0.47..8.64)	(-15.106..70.399)
Kin Binza Station	146.35	2 (1.28..4.87)	1.30 (0.41..3.13)	8.79 (-21.94..42.69)

4 Model evaluation

In this section we show the results of the model evaluation for the assessed region. The climate models are evaluated against the observations in their ability to capture:

1**. Seasonal cycles:** For this, we qualitatively compare the seasonal cycles based on model outputs against observations-based cycles (Figs A.2 & A.3). We discard the models that exhibit ill-defined peaks in their seasonal cycles. We also discard the model if the rainy season onset/termination varies significantly from the observations.

2. Spatial patterns: Models that do not match the observations in terms of the large-scale precipitation patterns (Figs A.4 & A.5) are excluded.

3. **Parameters of the fitted statistical models**. We discard the model if the model and observation parameters ranges do not overlap.

The models are labelled as 'good','reasonable', or 'bad' based on their performances in terms of the three criteria discussed above (Table 4.1). A model is given an overall rating of 'good' if it is rated 'good' for all three characteristics. If there is at least one 'reasonable', then its overall rating will be 'reasonable' and 'bad' if there is at least one 'bad'. The tables show the model evaluation results. In this study, given the relatively large number of models available, only

Table 4.1 *Evaluation results of the climate models considered for attribution analysis of Feb-March RX7day. For each model, the threshold for a 1-in-2-year event is shown, along with the best estimates of the Dispersion and Shape parameters are shown, along with 95% confidence intervals. Furthermore evaluation of the seasonal cycle and spatial pattern are shown in the appendix.*

Model / Observations	**Seasonal cycle**	**Spatial pattern**	**Sigma**	**Shape parameter**
TAMSAT			0.0570 (0.0420 ... 0.0670)	0.021 (-0.28 ... 0.29)
ERA5			0.0820 (0.0580 ... 0.109)	-0.25 (-1.1 ... -0.010)
CHIRPS			0.0680 (0.0480 ... 0.0800)	-0.074 (-0.26 ... 0.13)
CORDEX				
CanESM2_r1i1p1_SMHI-RCA4 historical-rcp85 (1)	good	reasonable	0.0818 (0.0617 ... 0.0976)	-0.33 (-0.54 ... -0.18)
CNRM-CM5_r1i1p1_CLMcom-CCLM4-8-17 historical-rcp86 (1)	reasonable	good	0.113 (0.0840 ... 0.129)	-0.14 (-0.41 ... 0.13)

CNRM-CM5_r1i1p1_SMHI-RCA4 historical-rcp87 (1)	reasonable	reasonable	0.0720 (0.0551 ... 0.0850)	-0.23 (-0.47 ... -0.058)
CSIRO-Mk3-6-0_r1i1p1_SMHI-RCA4 historical-rcp88 (1)	bad	bad	0.0777 (0.0654 ... 0.0877)	-0.18 (-0.50 ... -0.053)
EC-EARTH_r1i1p1_CLMcom-CCLM4-8-17 historical-rcp89 (1)	good	bad	0.151 (0.120 ... 0.181)	-0.28 (-0.60 ... -0.095)
EC-EARTH_r1i1p1_KNMI-RACMO22T historical-rcp90 (1)	bad	reasonable	0.0557 (0.0444 ... 0.0653)	-0.075 (-0.31 ... 0.097)
EC-EARTH_r1i1p1_MPI-CSC-REMO2009 historical-rcp91 (1)	bad	reasonable	0.0686 (0.0554 ... 0.0805)	-0.24 (-0.42 ... -0.089)
EC-EARTH_r1i1p1_SMHI-RCA4 historical-rcp92 (1)	good	reasonable	0.0752 (0.0588 ... 0.0874)	-0.26 (-0.54 ... -0.12)
GFDL-ESM2M_r1i1p1_SMHI-RCA4 historical-rcp93 (1)	good	good	0.0812 (0.0664 ... 0.0929)	-0.21 (-0.40 ... -0.044)
HadGEM2-ES_r1i1p1_CLMcom-CCLM4-8-17 historical-rcp94 (1)	reasonable	good	0.147 (0.117 ... 0.168)	-0.11 (-0.30 ... 0.081)
HadGEM2-ES_r1i1p1_KNMI-RACMO22T historical-rcp95 (1)	bad	reasonable	0.0449 (0.0324 ... 0.0529)	-0.024 (-0.18 ... 0.24)
HadGEM2-ES_r1i1p1_SMHI-RCA4 historical-rcp96 (1)	reasonable	reasonable	0.0779 (0.0653 ... 0.0895)	-0.28 (-0.50 ... -0.13)
IPSL-CM5A-MR_r1i1p1_SMHI-RCA4 historical-rcp97 (1)	good	reasonable	0.0714 (0.0574 ... 0.0824)	-0.22 (-0.39 ... -0.096)
MIROC5_r1i1p1_SMHI-RCA4 historical-rcp98 (1)	good	good	0.0592 (0.0491 ... 0.0686)	-0.39 (-0.62 ... -0.23)
MPI-ESM-LR_r1i1p1_CLMcom-CCLM4-8-17 historical-rcp99 (1)	good	good	0.136 (0.108 ... 0.156)	-0.22 (-0.50 ... -0.068)
MPI-ESM-LR_r1i1p1_MPI-CSC-REMO2009 historical-rcp100 (1)	bad	good	0.0671 (0.0561 ... 0.0773)	0.010 (-0.20 ... 0.18)
MPI-ESM-LR_r1i1p1_SMHI-RCA4 historical-rcp85 (1)	good	good	0.0774 (0.0655 ... 0.0890)	-0.38 (-0.84 ... -0.29)
NorESM1-M_r1i1p1_SMHI-RCA4 historical-rcp85 (1)	reasonable	reasonable	0.0800 (0.0631 ... 0.0921)	-0.28 (-0.45 ... -0.10)
HighResMIP				
CAM-MPAS-HR historicalSST-future (1)	reasonable	reasonable	0.171 (0.123 ... 0.204)	-0.17 (-0.49 ... 0.023)
CAM-MPAS-LR historicalSST-future (1)	reasonable	reasonable	0.191 (0.122 ... 0.240)	-0.33 (-0.68 ... -0.083)

CMCC-CM2-HR4 historicalSST-future (1)	bad	bad	0.101 (0.0707 ... 0.120)	-0.34 (-0.61 ... 0.032)
CMCC-CM2-VHR4 historicalSST-future (1)	bad	reasonable	0.128 (0.0872 ... 0.157)	-0.28 (-0.75 ... -0.10)
EC-Earth3P historicalSST-future (1)	good	reasonable	0.0905 (0.0604 ... 0.107)	-0.59 (-0.88 ... -0.12)
EC-Earth3P-HR historicalSST-future (1)	good	reasonable	0.0906 (0.0633 ... 0.111)	-0.39 (-0.73 ... -0.096)
FGOALS-f3-H historicalSST-future (1)	reasonable	reasonable	0.163 (0.0481 ... 0.191)	-0.23 (-0.60 ... 3.9)
HadGEM3-GC31-HM historicalSST-future (1)	reasonable	reasonable	0.147 (0.105 ... 0.177)	-0.30 (-0.61 ... -0.15)
HadGEM3-GC31-LM historicalSST-future (1)	reasonable	reasonable	0.157 (0.121 ... 0.188)	-0.15 (-0.60 ... 0.092)
HadGEM3-GC31-MM historicalSST-future (1)	reasonable	reasonable	0.152 (0.0898 ... 0.198)	-0.43 (-0.76 ... 0.064)
HiRAM-SIT-HR historicalSST-future (1)	reasonable	reasonable	0.0842 (0.0616 ... 0.101)	0.10 (-0.19 ... 0.43)
HiRAM-SIT-LR historicalSST-future (1)	bad	reasonable	0.139 (0.105 ... 0.170)	-0.38 (-0.82 ... -0.15)
MPI-ESM1-2-HR historicalSST-future (1)	good	reasonable	0.146 (0.111 ... 0.182)	-0.19 (-0.66 ... -0.0065)
MPI-ESM1-2-XR historicalSST-future (1)	good	reasonable	0.125 (0.0910 ... 0.154)	-0.11 (-0.39 ... 0.22)
NICAM16-7S historicalSST-future (1)	bad	reasonable	0.0921 (0.0660 ... 0.118)	-0.078 (-0.44 ... 0.18)
NICAM16-8S historicalSST-future (1)	bad	reasonable	0.0983 (0.0616 ... 0.126)	-0.28 (-0.65 ... 0.071)

5 Multi-method multi-model attribution

This section shows Probability Ratios and change in intensity ΔI between a past climate that is 1.3℃ cooler than now and the current climate for models that passed model evaluation and also includes the values calculated from the fits with observations. For the CORDEX-Africa ensemble we additionally show the results between the current climate and a future climate that is 1.3℃ warmer than now.

Table 5.1. Event magnitude, probability ratio and change in intensity for 2-year return period for Feb-March RX7day for observational datasets and each model that passed the evaluation tests. (a) from pre-industrial climate to the present and (b) from the present to 3℃ above pre-industrial climate.

Model / Observations	Threshold for return period 2 yr (mm/7day)				
		Probability ratio PR [-]	Change in intensity ΔI [˚C]	Probability ratio PR [-]	Change in intensity ΔI [˚C]
TAMSAT	103.41	70 (11 ... 2.1e+4)	28 (18 ... 41)		
ERA5	82.518	1.0 (0.080 ... 2.0e+3)	0.10 (-16 ... 18)		
CHIRPS	74.06	0.80 (0.55 ... 0.99)	-12 (-22 ... -0.65)		
CanESM2_r1i1p1_SMHI-RCA4 historical-rcp85 (1)	78	0.85 (0.65 ... 1.3)	-1.8 (-5.9 ... 2.0)	0.97 (0.86 ... 1.1)	-0.32 (-1.4 ... 0.64)
CNRM-CM5_r1i1p1_CLMcom-CCLM4-8-17 historical-rcp85(1)	1.1e+2	1.4 (0.72 ... 8.8)	4.9 (-5.7 ... 24)	1.0 (0.83 ... 1.3)	0.53 (-2.5 ... 4.4)
CNRM-CM5_r1i1p1_SMHI-RCA4 historical-rcp85(1)	77	0.72 (0.53 ... 2.0)	-3.7 (-11 ... 4.4)	0.82 (0.65 ... 1.0)	-1.7 (-3.4 ... 0.0076)
EC-EARTH_r1i1p1_SMHI-RCA4 historical-rcp85 (1)	93	2.5 (1.4 ... 9.9)	6.6 (2.6 ... 12)	1.4 (1.2 ... 1.5)	3.3 (2.0 ... 4.5)
GFDL-ESM2M_r1i1p1_SMHI-RCA4 historical-rcp85 (1)	76	1.8 (0.71 ... 24)	5.0 (-4.1 ... 16)	1.2 (0.96 ... 1.4)	1.8 (-0.42 ... 4.0)
HadGEM2-ES_r1i1p1_SMHI-RCA4 historical-rcp85 (1)	80	1.5 (0.91 ... 3.2)	3.3 (-0.93 ... 7.6)	1.0 (0.87 ... 1.1)	0.075 (-1.2 ... 1.4)
IPSL-CM5A-MR_r1i1p1_SMHI-RCA4 historical-rcp85 (1)	74	0.86 (0.60 ... 1.5)	-1.5 (-6.2 ... 3.2)	0.98 (0.85 ... 1.1)	-0.22 (-1.3 ... 0.90)
MIROC5_r1i1p1_SMHI-RCA4 historical-rcp85(1)	98	4.8 (1.3 ... ∞)	6.6 (1.7 ... 11)	1.4 (1.2 ... 1.5)	2.9 (1.8 ... 3.9)
MPI-ESM-LR_r1i1p1_CLMcom-CCLM4-8-17 historical-rcp85 (1)	1.0e+2	0.60 (0.52 ... 0.78)	-13 (-20 ... -5.2)	0.68 (0.51 ... 0.83)	-6.9 (-10 ... -3.6)
MPI-ESM-LR_r1i1p1_SMHI-RCA4 historical-rcp85 (1)	88	1.1 (0.76 ... 2.6)	1.2 (-3.0 ... 5.2)	1.0 (0.86 ... 1.2)	0.047 (-1.3 ... 2.1)

NorESM1-M_r1i1p1_SMHI-RCA4 historical-rcp85 (1)	82	1.2 (0.66 ... 4.0)	1.7 (-5.2 ... 9.1)	1.1 (0.97 ... 1.3)	1.5 (-0.36 ... 3.2)
CAM-MPAS-HR historicalSST-future (1)	61	1.3 (0.77 ... 3.0)	4.9 (-5.6 ... 17)	(...)	(...)
CAM-MPAS-LR historicalSST-future (1)	60	1.2 (0.72 ... 3.8)	3.7 (-9.9 ... 19)	(...)	(...)
EC-Earth3P historicalSST-future (1)	66	0.73 (0.59 ... 1.3)	-4.0 (-8.9 ... 2.1)	(...)	(...)
EC-Earth3P-HR historicalSST-future (1)	63	0.73 (0.59 ... 1.1)	-4.4 (-9.6 ... 1.1)	(...)	(...)
HadGEM3-GC31-HM historicalSST-future (1)	74	0.76 (0.56 ... 1.2)	-5.3 (-16 ... 3.2)	(...)	(...)
HadGEM3-GC31-LM historicalSST-future (1)	72	0.68 (0.51 ... 1.9)	-9.3 (-23 ... 9.8)	(...)	(...)
HadGEM3-GC31-MM historicalSST-future (1)	78	0.70 (0.54 ... 1.1)	-7.6 (-16 ... 1.9)	(...)	(...)
HiRAM-SIT-HR historicalSST-future (1)	67	1.1 (0.64 ... 2.7)	0.99 (-6.3 ... 9.4)	(...)	(...)
MPI-ESM1-2-HR historicalSST-future (1)	70	1.6 (0.70 ... 12)	7.6 (-7.6 ... 24)	(...)	(...)
MPI-ESM1-2-XR historicalSST-future (1)	64	2.5 (1.0 ... 39)	12 (0.52 ... 27)	(...)	(...)

6 Hazard synthesis

For the event definition described above, 7-day maximum February–May rainfall over the Ndjili river basin, we evaluate the influence of anthropogenic climate change on the such defined heavy rainfall by calculating the probability ratio as well as the change in intensity using the gridded data-products and climate models. Models which do not pass the evaluation described above are excluded from the analysis. The aim is to synthesise results from models that pass the evaluation along with the observations-based products, to give an overarching attribution statement.

Figure 6.1 shows the changes in probability and intensity for the observations (blue) and models (red). Before combining them into a synthesised assessment, first, a representation error is added (in quadrature) to the observations, to account for the difference between observations-based datasets that cannot be explained by natural variability. This is shown in these figures as white boxes around the light blue bars. The dark blue bar shows the average over the observation-based products. Next, a term to account for intermodel spread is added (in quadrature) to the natural variability of the models. This is shown in the figures as white boxes around the light red bars. The dark red bar shows the model average, consisting of a weighted mean using the (uncorrelated) uncertainties due to natural variability plus the term representing intermodel spread (i.e., the inverse square of the white bars).

Observation-based products and models are combined into a single result in two ways. Firstly, we neglect common model uncertainties beyond the intermodel spread that is depicted by the model average, and compute the weighted average of models (dark red bar) and observations (dark blue bar): this is indicated by the magenta bar. As, due to common model uncertainties, model uncertainty can be larger than the intermodel spread, secondly, we also show the more conservative estimate of an unweighted, direct average of observations (dark blue bar) and models (dark red bar) contributing 50% each, indicated by the white box around the magenta bar in the synthesis figures. More details can be found in Otto et al., (2024). Figure 6.2 shows the same, but for a 1.3C warmer climate.

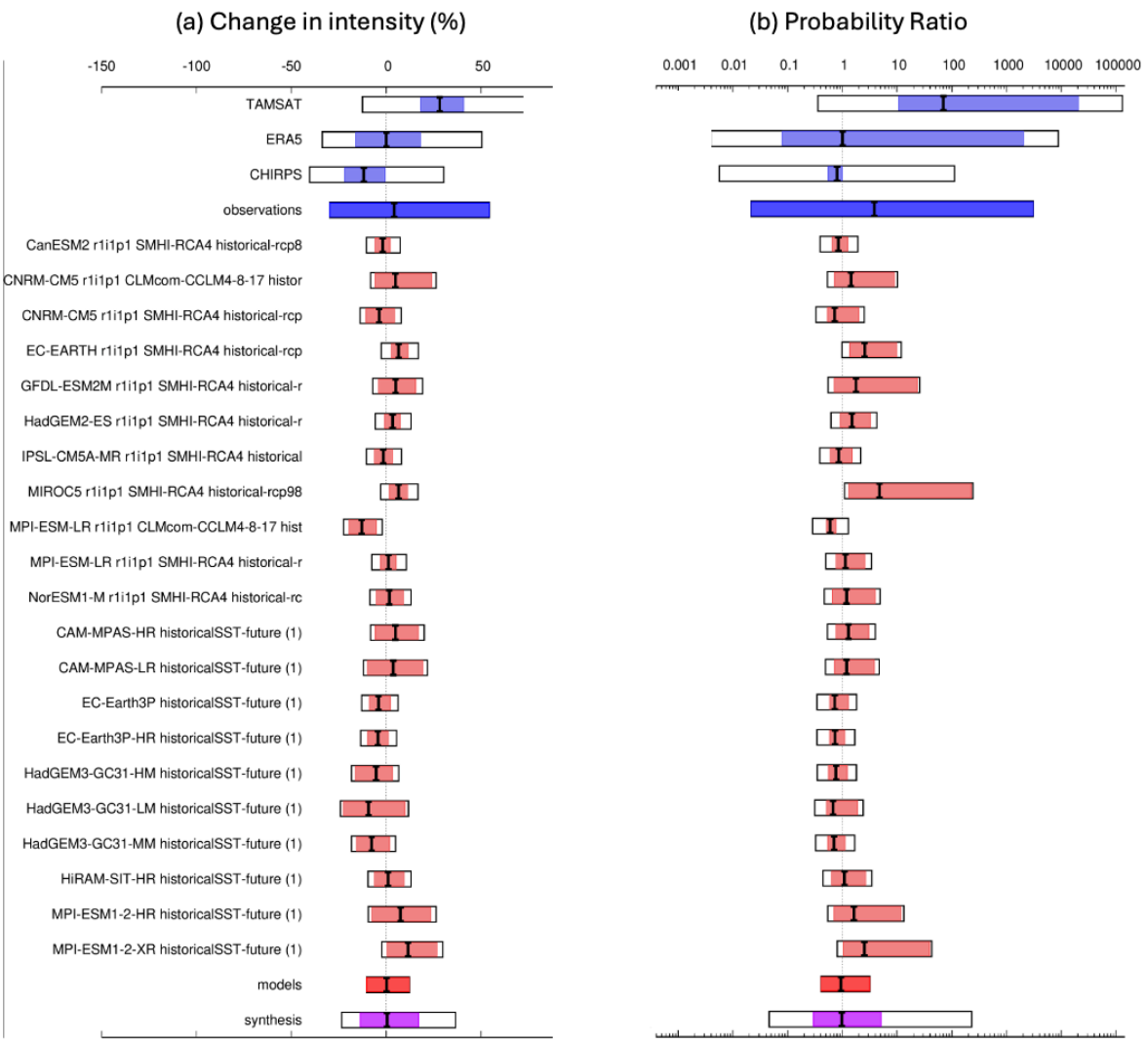

Figure 6.1: Synthesis of (a) intensity change and (b) probability ratios when comparing RX7day over the study region with a 1.3℃ cooler climate.

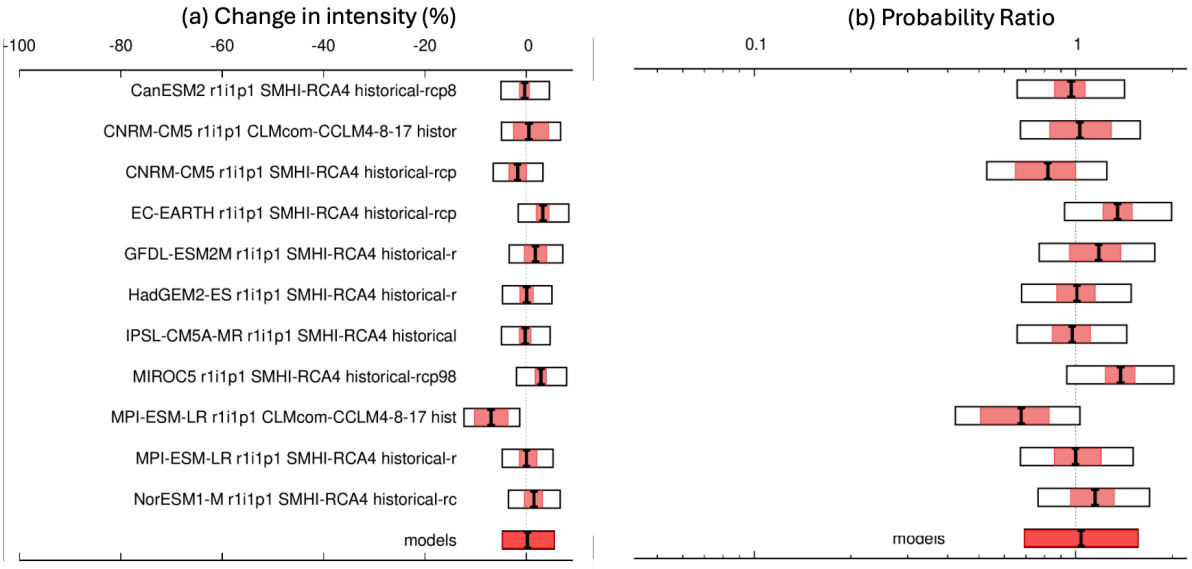

Figure 6.2: Synthesis of (a) intensity change and (b) probability ratios when comparing RX7day over

the study region with a 1.3℃ warmer climate.

As also discussed in section 3.2, the observational products show very different results that are incompatible with each other, highlighted by the large white boxes around the blue bars in figure 6.1. Therefore, some, or all of the observed products are clearly wrong. Given that the weather station data again shows a different behaviour we cannot exclude a data set or identify which ones are clearly wrong. Hence, while the synthesised observational results show no change as the best estimate this does not mean that there is no change. Without trustworthy observations to evaluate the climate models, the situation is similar: while the synthesised result for the models as well as overall is centred around zero, this does not mean that we can exclude climate change to be an important driver of more frequent and intense heavy rainfall events. We thus conclude that we cannot provide an attribution statement, but that the possibility of an important role of climate change can also not be excluded and thus need to be included in adaptation and resilience planning.

7 Vulnerability and Exposure

The April 2025 floods in western and central DRC exposed underlying social and structural conditions that continue to shape the country's vulnerability to climate-related hazards. Kinshasa, the capital of the DRC, has been heavily impacted by the floods following heavy rainfall. News reports indicate that almost half of the city of Kinshasa (26 districts) have been affected by the floods, submerging the main road to the airport and with the outskirts of the poorest neighborhoods of Kinshasa hit the hardest given its proximity to rivers beds (BBC, 2024). Roads and houses have been damaged, including the main road to the airport. Access to drinking water is not available in at least 16 communes of the city due to submerged water facilities (NPR, 2025).

The floods occurred in a region marked by geographic contrasts and demographic change. Many cities in the Congo River Basin (CRB) are located near the major rivers and tributaries, with 39 million people living within 10 km of one in the CRB (Trigg et al., 2020). Kinshasa, the capital, sits at the intersection of steep hills and low-lying floodplains along the Congo and N'Djili rivers in the far west, creating sharp variation in elevation and land use. Third-largest metropolitan area in Africa, the capital is currently home to about 18 million people, growing at an annual rate of 4.38% with urban densities reaching as high as 27,000 people per km2 (World Population Review, n.d.). With over 75% of the city households classified as poor (Global Data Lab, n.d.), the majority of Kinshasa's population lives in informal settlements that have expanded rapidly into flood-prone zones - conditions that exacerbate vulnerability even during moderate rainfall. Central DRC, on the other hand, is predominantly rural, with dispersed settlements, dense forested areas under pressure from subsistence agriculture and logging, and limited access to formal infrastructure. Across both contexts, population growth and land conversion are reshaping landscapes in ways that heighten flood risk.

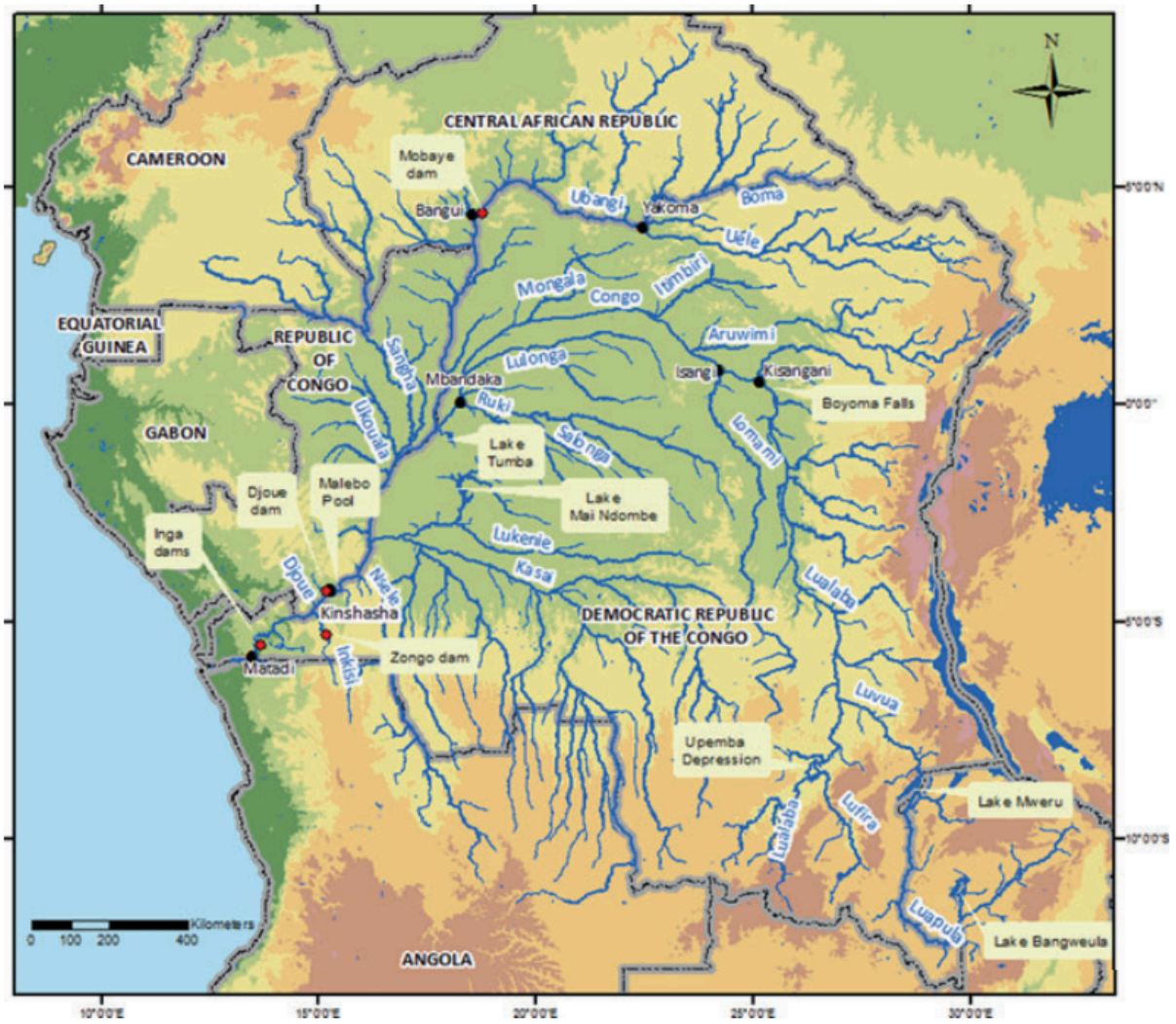

Figure 7.1: *Map of the Congo River Basin. Source: Harrison et al. (2016).*

Although this study focuses on western and central provinces, national patterns of displacement, governance strain, and economic instability - partly driven by prolonged conflict in the east - have ripple effects that shape conditions across the country, including in the capital. These challenges are further shaped by structural pressures linked to natural resource extraction. Eastern DRC hosts some of the world's richest deposits of cobalt and other critical minerals (Gulley, 2022; Lubaba Nkulu et al., 2018), which, while economically significant, have also contributed to persistent insecurity and competition over land and control. Over the past years, eastern DRC - particularly North Kivu - has experienced a rapidly evolving and devastating conflict, involving multiple armed actors, displacing over 1.6 million people and leaving millions more dependent on humanitarian assistance (IFRC, 2024). While concentrated in the east, this instability places additional pressure on national systems, particularly as displaced populations move westward and as humanitarian and government capacity is streteched thin (Mugisho et al., 2024). Kinshasa, historically a destination for migrants and those seeking safety or opportunity, has continued to absorb new arrivals from conflict-affected areas, further intensifying demand for services, housing, and jobs.

In this context, even short-duration or localized flood events can trigger wide-reaching impacts. Understanding these interconnected drivers is essential to assessing current risk, and to anticipating

how vulnerability and exposure may evolve as rainfall events intensify and structural stressors persist across the DRC.

7.1 Land-use changes

Land-use change and environmental degradation are key factors shaping flood vulnerability in Kinshasa and across central DRC. The replacement of natural vegetation with compacted surfaces - such as bare soil, informal roads, and trampled grounds - has significantly reduced infiltration and increased surface runoff (Moeyersons et al., 2015). In Kinshasa, runoff coefficients - how much rainfall flows over the surface rather than being absorbed by the ground - reach up to 96% on over-compacted roads, while vegetated or cultivated plots with full soil coverage produce negligible runoff (Moeyersons et al., 2015). Even partially covered areas, such as bare soil with lichen crusts, generate intermediate runoff (about 40%), highlighting the sensitivity of runoff response to ground cover quality.

Increased runoff intensifies both erosion and flood risk. Concentrated overland flow, especially on steep slopes, leads to gully formation and sediment transport. In Kinshasa, this process has contributed to the development of hundreds of large urban gullies - some over 100m long - that not only degrade terrain, but also act as flood conduits, accelerating water flow toward downstream communities (Lutete Landu et al., 2025). Erosion in these contexts compromises slope stability and overwhelms natural retention systems, further amplifying flood peaks.

In and around Kinshasa, deforestation is driven by intersecting pressures linked to rapid population growth, energy demand, and expanding subsistence needs (Re Soil Foundation, 2022). With most households in the capital relying on charcoal and fuelwood for cooking, biomass harvesting remains a leading cause of forest loss (Butler, 2020). This demand, combined with slash-and-burn agriculture on the city's periphery, contributed to steady degradation of natural vegetation cover. Logging - both legal and informal - also plays a role, with access roads facilitating additional land-use change and resource extraction (Re Soil Foundation, 2022). These processes weaken natural hydrological regulation, particularly on the city's exposed slopes, where forest loss undermines infiltration, destabilizes soils, and accelerates runoff. Over time, this cumulative deforestation has diminished the landscapes's ability to absorb heavy rains, amplifying both erosion and flood risk. In Kinshasa's low-lying neighborhoods, sediment from upland erosion also clogs drainage channels, compounding flood impacts during peak rainfall.

Beyond Kinshasa, erosion mapping and ecological studies highlight similar dynamics across central DRC. Over 25,000 hectares of Kinshasa are classified as highly erosion-prone - mainly in elevated, sparsely vegetated zones (Kabantu et al., 2018). Research from the Yangambi region, while outside the study's immediate scope, illustrates how forest fragmentation driven by shifting cultivation and settlement expansion weakens watershed buffering capacity. Landscape indicators, such as disturbed forest edge density and cropland patchiness, have been found to correlate with altered runoff and declining water quality (Chishugi et al., 2021). These patterns reflect environmental transformations effecting both rural watersheds and downstream urban systems, underscoring the regional relevance of land cover change to flood risk.

While these land-use dynamics shape the physical drivers of flood risk, the distribution of exposure is deeply influenced by how space is organized, regulated, or informally occupied. Urban layout, infrastructure, and planning practices play a decisive role in shaping who is most vulnerable and why.

7.2 Urban planning and informality

Kinshasa is one of the most populated cities in the world, with estimates of close to 18 million with projections to double within the next 20 years (World Population Review World Bank, 2021). Urban planning has been based on the city's layout under colonial occupation with the last development frameworks dating back to 1967 (Mufungizi & Akilimali, 2024). Hence, large accumulations of informal settlements (75% of urban population) have formed with little green spaces to absorb flood waters (see figure 7.2) (Núnez and Jessse, 2025 World Bank, 2021).

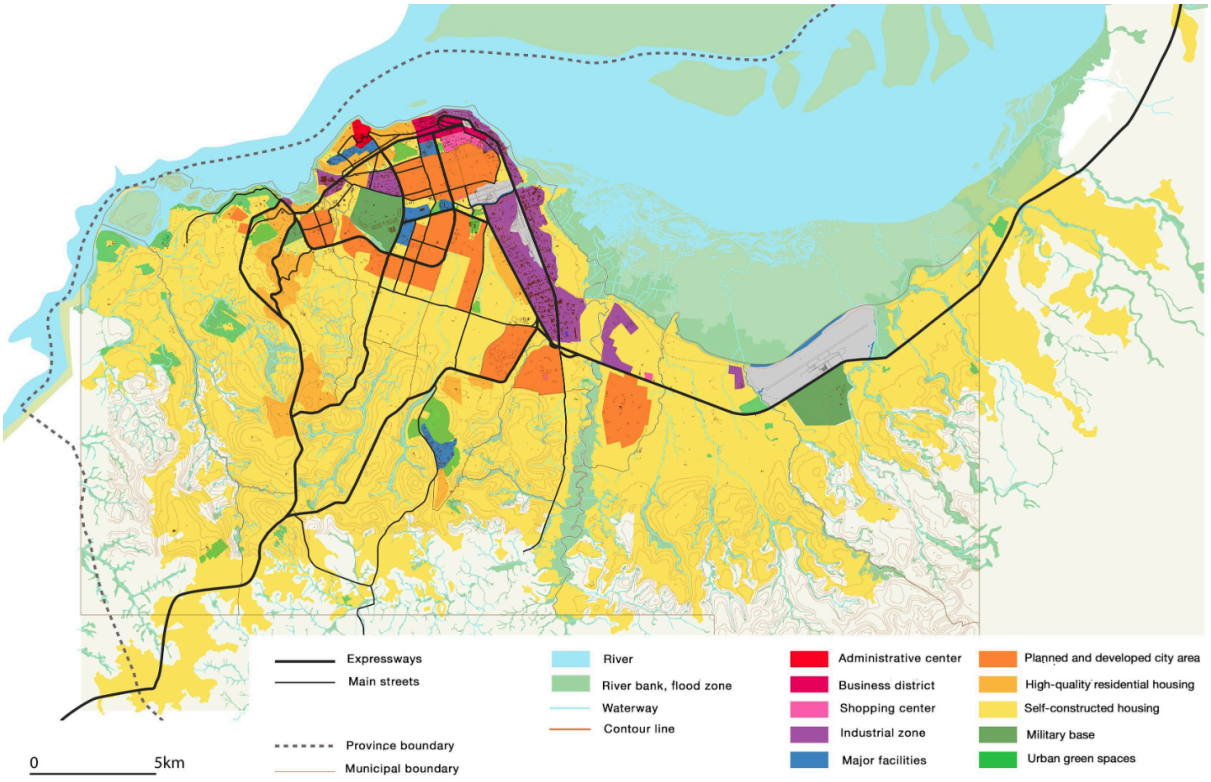

Figure 7.2: *Types of land use, produced for the Kinshasa Metropolitan Area Strategic Master Plan (Guérin et al., 2013, presented in Bédécarrats et al., 2019).*

The pressure on the need for housing pushes the population to build in major river beds during dry seasons, making flood impacts worse (Mufungizi & Akilimali, 2024,Nsokimieno et al., 2014). Historically, flood impacts are concentrated in neighbourhoods along the riverside, and peri-central neighbourhoods with high population density and precarity (Malumba, 2024). Neighborhoods such as Kingabwa, Kalamu, Matete, and Limete - located along the N'Djili, Yolo, and Kalamu rivers - are particularly affected, with informal settlements often built without adequate drainage or land regulation (Malumba, 2024). High densities, fragile housing, and poor waste management increase

both physical exposure and the risk of disease outbreaks during floods, including malaria, typhoid, and diarrhoea. Vulnerable groups such as children, older adults, and chronically ill individuals are disproportionately affected (Malumba, 2024). These areas are further characterised by a lack of sewerage, drainage systems, and waste disposal systems (Nsokimieno et al., 2014). Many drainage channels, where they exist, are often obstructed by solid waste (DRR Network of African Journalists, 2023; Kang et al., 2023). In low-lying neighborhoods, this has led to repeated flooding even during moderate rainfall, highlighting the compounding impact of informality, service gaps, and physical geography.

A study from 2019 shows that the majority of the population in Kinshasa is exposed to floods (58%) with most affected areas in Kalamu, Mont-Ngafula and Limete, which is in direct proximity to the flooded Ndjili river in the east (UNDP, 2023). Results from an impact analysis conducted by the Red Cross and University of Kinshasa (2021), confirm flood impacts in various neighbourhoods in Limete, due to their close proximity and low elevation compared to the riverbed (Imwangana et al., 2021). Additionally, areas along the Ndjili river have been identified as hotspots for vector borne and water borne diseases such as malaria and diarrheal diseases, that are being promoted through stagnant flood waters, lacking sewage and open waste disposal (Malumba, 2024). Furthermore, access to essential services is among the lowest in all major African cities and while 68% of the population in Kinshasa have access to piped water World Bank, 2021, news report show that drinking water is not available in at least 16 communes of the city due to submerged water facilities (NPR, 2025) and the access to safe water, electricity, and toilets is especially low in precarious areas of the affected outskirts (Nsokimieno et al., 2014).

Kinshasa is crossed by the Congo River, but limited wastewater infrastructure means much of the city's effluent is discharged directly into rivers or open drains. Currently, only 5.5% of the population is connected to a sewer system, which itself captures merely 40% of the city's daily water usage. The remaining wastewater is typically released into open wells or onto the streets. This inadequate sanitation infrastructure not only exacerbates river pollution but also poses serious public health risks through the spread of waterborne diseases linked to untreated wastewater (Milot, 2019). Congolese scientists report high levels of faecal contamination in urban watercourses (Booty, Makumeno, 2025), and the overflow of one of Kinshasa's most polluted streams raises serious public health concerns.

Additional vulnerabilities arise due to high levels of poverty, unemployment and social inequity. Disaster impacts are seen due to existing conditions of poverty (Raju, Boyd & Otto, 2022; Alcantara-Ayala, 2022). Poverty and unemployment rates in informal settlements are above 90% and are among the highest in the world (Nsokimieno et al., 2014). Poverty has been exacerbated through the Covid-19 pandemic and inflation. Furthermore, due to continuous loss in value of the Congo Franc, the American Dollar has become an informal second currency, however it remains inaccessible for the lowest income groups, widening the inequalities. Social structures reinforce poverty with larger households being significantly poorer and female headed households being poorer than male headed households (World Bank, 2021). During floods, poverty and loss of employment increases due to inaccessibility of infrastructure, which translates to economic losses of 1.2 million USD per day among local commuters (He et al., 2021).

The challenges described above - rapid, unplanned growth, weak infrastructure, and high levels of informality - significantly constrain flood resilience. These pressures compound existing risks and

limit the capacity for mitigation. The following section explores how these vulnerabilities intersect with flood management systems across Kinshasa and the wider Congo Basin.

7.3 Flood risk management

The DRC has developed a range of frameworks to address disaster risk reduction (DRR) and flood management. The National Strategy and Action Plan for Reducing Natural Risks and Disasters (2017-2023) outlines nine priority areas, including the official recognition of DRR, implementation of institutional mechanisms, and strengthening of disaster preparedness and response activities at the national level. Additionally, the DRC's National Adaptation Plan (2022-2026) emphasizes integrating climate change adaptation into national development planning, with a focus on enhancing institutional capacity and coordination among stakeholders. Further, validated in 2024, a new national urban planning and construction code offers a framework for better integrating land use and hazard exposure, but has yet to be operationalized in Kinshasa (Radio Okapi, 2024).

Efforts to integrate catchment-based thinking into flood risk management are emerging (Cap-Net, n.d.). In river basins such as the Lukaya, government agencies and development partners have piloted integrated water resource management (IWRM) activities, including reforestation, erosion control, and participatory monitoring networks, to reduce runoff and improve coordination between upstream and downstream communities (UNEP, 2017).

In 2018, severe flooding in Kinshasa resulted in 51 fatalities, affected approximately 16,000 people, and caused damages and losses estimated at US$76 million. A rapid Post-Disaster Assessment conducted by the Government of the DRC and Kinshasa Municipality, with support from the Global Facility for Disaster Reduction and Recovery (GFDRR) and the World Bank, identified the absence of early warning systems as a major contributing factor to the high human toll and widespread impact (CREWS, 2018).

The DRC has made progress in developing early warning systems (EWS), especially in high-risk watersheds such as the N'Djili and Kalamu basins. Supported by the CREWS initiative and other partners, EWS infrastructure now includes a network of rain and river gauges, delivering updated forecasts every three hours (CREWS, n.d.). Alerts are disseminated through radio, television, and mobile channels (WMO, n.d.), reaching an estimated 300,000 people (CREWS, n.d.). Community-based networks coordinated by local actors and organizations such as UNICEF and the Catholic Church (CRS) help spread alerts in areas with limited communication infrastructure (CRS & UNICEF, 2017; CRS, n.d.). Though gaps in coverage persist, particularly across remote or informal settlements, these systems have enabled faster decision-making and improved coordination across civil protection agencies (CRS & UNICEF, 2017; CREWS, n.d.).

In Kinshasa, flood risk remains high due to rapid urban growth, and limited basic services and infrastructure coverage. Targeted risk reduction efforts have focused on the N'Djili River watershed, where World Bank-supported projects have included risk assessments, drainage rehabilitation, slope stabilization through vegetation, and dredging of high-risk channels (World Bank, 2023). For example, the Kin-Elenda project aims to strengthen flood resilience in the capital by improving hydrometeorological data collection and early warning systems. It promotes inclusive, risk-informed planning and enhances coordination among agencies including MettelSat, INERA, and the Civil

Protection Department, while linking local data systems with global platforms to better alerts as well as emergency response (World Bank, 2023).

7.4 Governance

Following its colonial legacy, the Democratic Republic of the Congo (DRC) continues to face significant challenges in climate governance and land-use planning, rooted in a legacy of weak legal and institutional frameworks. In particular, the absence of a coherent system for land-use planning has hindered sustainable land governance and contributed to recurrent land conflicts. Developing such frameworks, especially through inclusive processes involving civil society, offers a strategic opportunity to strengthen land tenure security and reduce tensions. This is especially critical for the DRC's most disadvantaged communities, who largely reside in forested areas and depend on land for their livelihoods. Clarifying their land use and governance rights is essential for promoting community-led conservation efforts and reinforcing peace, security, and resilience at the local level (The Land Writes, 2023).

As noted by environmental researcher Prof. Cush Ngonzo Luwesi, the absence of a national climate strategy has led to "a lack of cohesion and unifying objectives" (Gabbatiss, Viglione, 2024). While the Environmental Protection Law (Journal Officiel de la République Démocratique du Congo, 2011) mandates the state and provinces to adopt necessary climate adaptation measures, implementation remains limited. Nevertheless, some progress is underway: the DRC Government, in collaboration with the United Nations Development Programme (UNDP), is in the process of developing the country's first disaster risk reduction (DRR) policy. Although the 2013 Poverty Reduction Strategy highlights climate adaptation and disaster risk management (DRM) as central priorities, there is still no systematic tracking of government spending on DRR.

Moving forward, key priorities include enhancing hazard monitoring and forecasting, integrating risk knowledge into planning and decision-making, strengthening early warning systems and contingency planning, and building institutional capacity for effective DRM (GFDRR, 2024).

V&E Conclusion

While the physical hazard was significant, the scale of human impact was largely driven by long-standing vulnerabilities and patterns of exposure. In Kinshasa and surrounding areas, flood risk is amplified by rapid population growth, limited infrastructure coverage, and high reliance on informal systems - particularly in areas where critical services such as drainage, healthcare, and electricity remain inconsistent or difficult to access.

Population pressure has driven the expansion of settlements into flood-prone areas, often without adequate planning or protective infrastructure. At the same time, the loss of vegetative cover and poor waste management have further eroded the capacity to absorb and respond to flood hazards. These risks are expected to aggravate, as Kinshasa's population - already about 18 million - continues to grow at over 4% annually, along with rainfall extremes likely becoming more intense under a changing climate.

Data availability

All time series used in the attribution analysis are available via the Climate Explorer.
%FOR DATA THAT ISN'T, data is available upon request, CONTACT...:

References

All references are given as hyperlinks in the text.

Appendix

A.1 Model evaluation tables

%only for large ensembles if not totally shown in sect 4.

A.2 Additional details

%only if needed for extra figures